Evidence of macroscopic quantum tunneling from both wells in a φ Josephson junction

R. Menditto,[1] M. Merker,[2] M. Siegel,[2] D. Koelle,[1] R. Kleiner,[1] and E. Goldobin[1]
[1]*Physikalisches Institut and Center for Quantum Science in LISA$^+$, Universität Tübingen, Auf der Morgenstelle 14, D-72076 Tübingen, Germany*
[2]*Institut für Mikro- und Nanoelektronische Systeme, KIT, 76187, Karlsruhe, Germany*

(Received 15 February 2018; published 16 July 2018)

We study Nb-AlO$_x$-Nb Josephson junctions (JJs) with a phase-discontinuity κ created by a pair of current injectors attached to one of the Nb electrodes. For $\kappa \approx \pi$ the Josephson potential energy U as a function of the average phase ψ across the JJ has the form of a 2π-periodic double-well potential. Thus, the device behaves as a φ JJ with degenerate ground state phases $\psi = \pm\varphi$ (the value of φ depends on the system parameters). Experimentally, the existence of two wells of the potential is confirmed by the observation of two different critical currents $I_{c\pm}$, corresponding to the escape from different wells. We investigate the escape of the Josephson phase from *both* wells by collecting statistics of the switching currents. The histogram of switching current exhibits two peaks corresponding to $I_{c\pm}$. The dependence of the width σ_+ and σ_- of each peak on the bath temperature T indicates the transition from thermal activation to macroscopic quantum tunneling (MQT) at $T^\star \approx 260$ mK as T decreases. We argue that the observed saturation value of σ_+ and σ_- below $T^\star$ is indeed related to quantum tunneling rather than to parasitic noise in the system, as the histogram width can be reduced by tuning the value of κ away from π. The comparison of the experimental escape rate Γ with theoretical predictions further confirms MQT of the phase ψ from *both* wells.

DOI: 10.1103/PhysRevB.98.024509

I. INTRODUCTION

φ Josephson junctions (JJs) are fascinating novel devices showing unusual physics [1–3] and offering a functionality suitable for applications in superconducting electronics. The key property of a φ JJ is that its Josephson energy $U(\phi)$ has the form of a 2π-periodic double-well potential, with minima at the values of the Josephson phase $\phi = \pm\varphi \bmod 2\pi$. A nonzero ground state phase allows one to use φ JJs as phase batteries, similar to π JJs [4,5]. The two ground states are degenerate and can be used to store information [6], as demonstrated recently [7]. The degeneracy can be lifted upon application of, e.g., a magnetic field, and the Josephson energy profile may become reflection asymmetric. This property is useful to construct ratchets [8] that attracted a lot of attention in the last years [9]. The φ JJs were not investigated in the quantum domain up to now. Thus, the investigation of macroscopic quantum tunneling (MQT) is the topic of immediate interest.

The first experimental realization of a φ JJ was based on a 0-π JJ in a superconductor-insulator-ferromagnet-superconductor (SIFS) heterostructure with a tailored ferromagnetic barrier [10]. The experiment followed the theoretical proposal that a 0-π JJ with somewhat asymmetric 0 and π segments (lengths $L_0 \neq L_\pi$ or critical current densities $j_{c0} \neq j_{c\pi}$) results in a φ JJ, if parameters are carefully chosen [11–13]. The existence of two degenerate ground states was successfully demonstrated by detecting two critical currents, I_{c+} and I_{c-}, corresponding to the escape of the phase from the $+\varphi$ and $-\varphi$ wells of the potential. Further investigations and the first applications of the SIFS-based φ JJs were reported [2,3,7,8]. However, the macroscopic quantum properties of a φ JJ remain uninvestigated.

The SIFS based φ JJs at the present stage of technology are *not* very suitable for MQT experiments. First, due to the presence of the ferromagnetic layer, they have a rather low critical current density j_c (the world record is $\sim 50 \ldots 60$ A/cm^2 in the π state [10,14]), that leads to a thermal-to-quantum crossover temperature $T^\star \sim 20 \ldots 30$ mK—i.e., at the limit of available dilution refrigerators. Second, SIFS φ JJs have a relatively high damping even at mK temperatures [3], which will result in a strong decoherence.

In the current work, we implement a φ JJ based on conventional Nb-AlO$_x$-Nb SIS technology, where the phase discontinuity is created by means of two tiny current injectors attached to one of the Nb electrodes of the junction [15–18] at a position slightly shifted from its center (Fig. 1). The injectors have a width $W_{\rm inj}$ and are separated by a distance $W_{\rm d}$. In order to have a steplike phase discontinuity, the injector dimensions have to be chosen in such a way that $2W_{\rm inj} + W_{\rm d} \ll \lambda_J$, where λ_J is the Josephson penetration depth. The current $I_{\rm inj}$ flowing through the injectors twists the phase $\phi(x)$. Consequently $\phi(x)$ changes from 0 to κ between the injector leads. The value of κ is proportional to $I_{\rm inj}$, thus a π discontinuity can be created [17] by applying the proper $I_{\rm inj} = I_{\rm inj}^{\kappa=\pi}$.

Such injectors were already used in the past to realize 0-π or, more generally, 0-κ JJs for the investigation of integer [15,16,19,20] and fractional Josephson vortices [17,18,21,22]. Now, we demonstrate that a similar device can be used to build a junction that can be turned from a 0 into a φ JJ by simply controlling the current $I_{\rm inj}$ applied to the injectors [23]. The tunability of the phase discontinuity turns out to be a powerful tool for measurements in the quantum domain, since it allows us to rule out effects due to parasitic noise in our system.

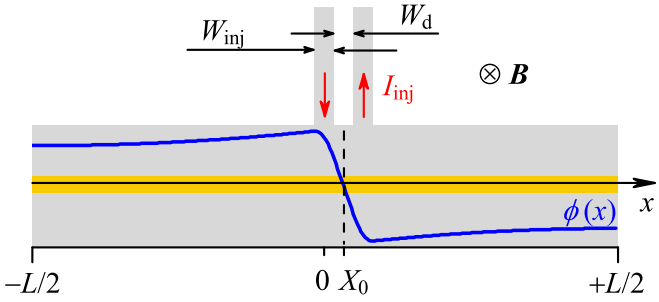

FIG. 1. Sketch of the investigated Josephson junction with two current injector leads attached on the top electrode. The blue line represents the spatial variation of the phase along the junction length.

In the following, we introduce the model used to describe and numerically simulate a JJ with a phase discontinuity induced by current injectors. Results are compatible with the ones obtained from the effective model for a short JJ with steplike discontinuity presented in [23]. However, here, we take into account the finite size of the injectors. We show simulations of the energy of the junction as a function of various parameters and discuss the results. Further, we present first characterization in the classical regime and subsequently statistics of *both* switching currents of our φ JJ in the quantum limit. The dependences of the widths $\sigma_\pm$ of both histograms vs temperature and injector current, together with the calculation of the escape rate Γ, are shown and the proofs of MQT are provided.

II. THE MODEL

We consider a JJ of normalized length $l = L/\lambda_J$ in the x direction and a normalized width $w = W/\lambda_J \ll 1$ in the y direction. The JJ is one dimensional (1D) in the sense that the phase ϕ, currents, and other quantities only depend on x. The JJ is equipped with a pair of current injectors of width $w_{inj} = W_{inj}/\lambda_J$ and distance $w_d = W_d/\lambda_J$ from each other, that are connected to the top electrode of the junction at a position $x_0 = X_0/\lambda_J$, see Fig. 1. In this paper, we will describe the case $x_0 \geqslant 0$. The opposite configuration ($x_0 < 0$) is analogous. In such a system, the dynamics of the Josephson phase $\phi(x,t)$ can be modeled by the 1D sine-Gordon equation

$$\phi_{xx} - \phi_{tt} - \sin\phi = \alpha\phi_t - \gamma - \gamma_{inj}(x), \tag{1}$$

where the subscripts x and t denote the derivatives with respect to the coordinate x and the time t, $\alpha = 1/\sqrt{\beta_c}$ is the damping parameter ($\beta_c = 2\pi j_c r^2 c/\Phi_0$ is the McCumber-Stewart parameter, where j_c is the the critical current density of the junction, c is its barrier's capacitance per area, and r is the junction resistance times area and the magnetic flux quantum $\Phi_0 \approx 2.068$ fWb), $\gamma = j/j_c$ is the normalized bias current density, and $\gamma_{inj}(x)$ is the injector current density normalized in the same way. Note that the spatial average of γ_{inj} on the whole JJ length is $\langle\gamma_{inj}(x)\rangle = 0$ as the injector current does *not* pass through the barrier, but rather injected and extracted to/from the top electrode. In Eq. (1), the spatial coordinate x is normalized to λ_J and the time t is normalized to the inverse of the Josephson plasma frequency $\omega_p^{-1} = c\Phi_0/(2\pi j_c)$. The injector current density distribution is related to the phase discontinuity κ as

$$\gamma_{inj}(x) = \begin{cases} \frac{\kappa}{w_{inj}(w_{inj}+w_d)} & x_0 - \left(w_{inj} + \frac{w_d}{2}\right) < x < x_0 - \frac{w_d}{2}, \\ 0 & x_0 - \frac{w_d}{2} < x < x_0 + \frac{w_d}{2}, \\ -\frac{\kappa}{w_{inj}(w_{inj}+w_d)} & x_0 + \frac{w_d}{2} < x < x_0 + \left(w_{inj} + \frac{w_d}{2}\right). \end{cases} \tag{2}$$

The total normalized current injected/extracted from each injector is, therefore, $i_{inj} = \kappa/(w_{inj} + w_d)$. In physical units $I_{inj} = \kappa(j_c\lambda_J^2 W)/(W_{inj} + W_d)$. Thus, $\kappa \propto i_{inj} \propto I_{inj}$.

In the case of a perfect κ discontinuity ($w_{inj} \to 0$ and $w_d \to 0$) $\gamma_{inj} \to \kappa\delta'(x) = -\kappa\delta(x)/x$, i.e., γ_{inj} looks like two oppositely oriented δ functions at $x = \pm 0$. We will call this limit of a perfect steplike discontinuity the limit of "δ-like injectors."

The phase profile $\phi_{inj}(x)$ imprinted by the injectors is defined by doubly integrating Eq. (2) over x. For the numerical solution of Eq. (1), it is more convenient to introduce the phase

$$\mu(x,t) = \phi(x,t) + \phi_{inj}(x) + 2\pi f x, \tag{3}$$

where $f = \Phi/\Phi_0$ is the normalized externally applied magnetic flux. The physical applied flux is defined as $\Phi = B \cdot \Lambda \cdot L$, where $\Lambda \approx 2\lambda$ (λ is the London penetration depth) and B is the magnetic field applied perpendicular to the plane of Fig. 1. Equation (1) can be rewritten in terms of $\mu(x,t)$ as:

$$\mu_{xx} - \mu_{tt} - \sin[\mu - \phi_{inj}(x) + 2\pi f x] = \alpha\mu_t - \gamma. \tag{4}$$

From Eq. (4), we can determine the effective normalized current-phase relation (CPR) $\gamma_s(\psi)$, where we defined $\psi \equiv \langle\mu(x)\rangle$—the average phase across the device. In accordance with Eq. (3), the phase ψ is related to $\langle\phi(x)\rangle$, which is the phase visible by external circuitry, as $\langle\mu(x)\rangle = \langle\phi(x)\rangle + (1 + X_0/L)\kappa/2$. To find $\gamma_s(\psi)$ we use two approaches. In the first one (dynamical method) the supercurrent is reconstructed from the time evolution of the phase $\mu(t)$ that we obtain by setting a finite bias $\gamma \gtrsim \gamma_c$, which brings the junction into the voltage state ($\mu_t > 0$). The second approach (static method) is based on the calculation of the average phase $\langle\mu\rangle$ of the static solution for different values of the bias. With this method only the stable part of the CPR can be scanned. The unstable part, corresponding to the regions near the local maxima of the energy, cannot be obtained. The comparison of the CPRs obtained with the two approaches shows a rather good match in the stable region, as visible in Fig. 2(a) (continuous lines). Once the effective CPR is found, the potential energy $U(\psi)$ of the JJ can be easily derived from it, since $\gamma_s(\psi) = \partial U/\partial\psi$. Below, we show simulations of the energy $U(\psi)$ of the device from Fig. 1, calculated using the dynamical method.

To this purpose, we considered $l = 2$, $w_{inj} = w_d = 0.06$, and $x_0 = 0.02$, because they are close to the experimental values. In Fig. 2(b), the potential $U(\psi)$ for $\kappa = 0, \pi$ is displayed. When $\kappa = 0$, the JJ is in the 0 state and the potential changes as $\sim(1 - \cos\psi)$ with minima at $\psi = 2\pi n$, with n an integer. As κ approaches π, two minima develop within every 2π period in the potential at $\psi = \pm\varphi$. The value of φ depends on the geometry of the junction.

This result generally confirms the theoretical predictions made for JJs with a perfect discontinuity [23]. However, one

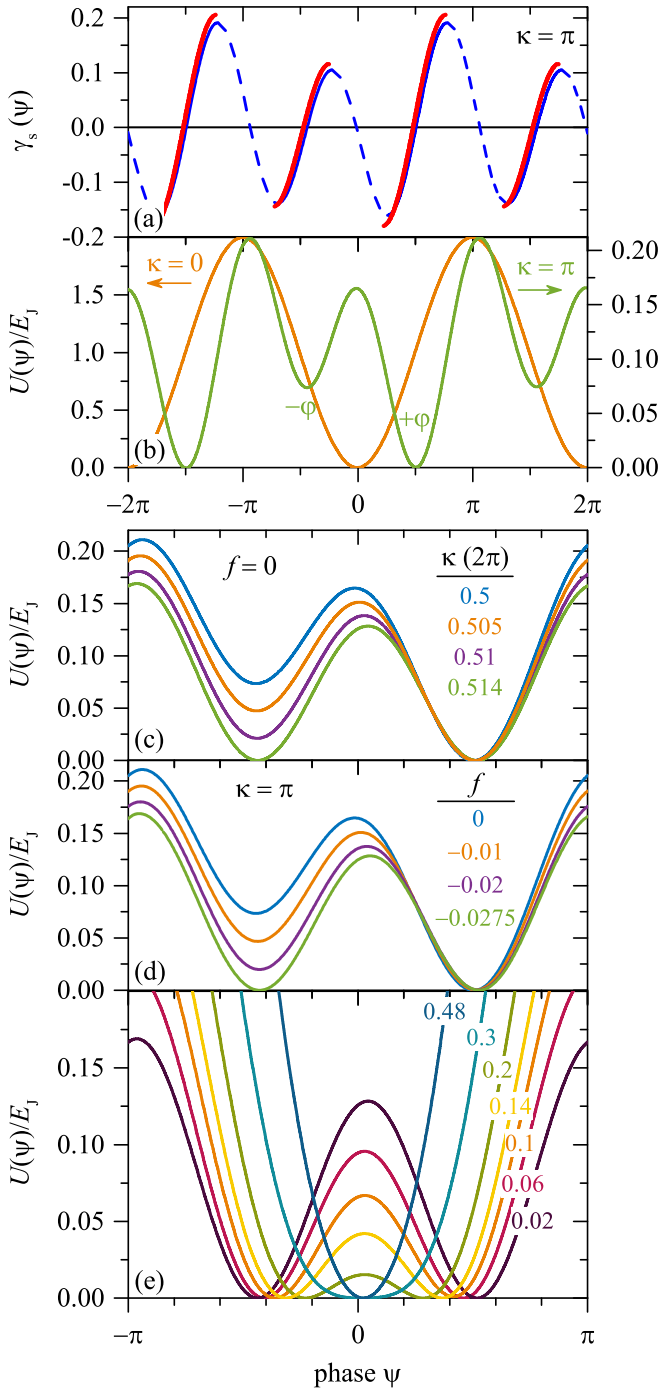

FIG. 2. (a) The CPR of the simulated JJ for $\kappa = \pi$ calculated with the dynamical method (blue) and with the static method (red). The dotted line represents the unstable part of the CPR. (b) Josephson potential $U(\psi)$ (normalized to the Josephson energy $E_J = I_c\Phi_0/2\pi$) for $\kappa = 0$ and $\kappa = \pi$. At $\kappa = \pi$ the wells have different depths, but this can be tuned by either $\kappa/2\pi$ (c) or f (d). (e) $U(\psi)/E_J$ for different injector positions x_0 indicated by the numbers. For each curve, the phase discontinuity κ is adjusted to κ_{sym}, $f = 0$.

can note some differences. For a perfect phase discontinuity, the potential $U(\psi)$ is symmetric at $\kappa = \pi$ and becomes asymmetric at $\kappa \neq \pi$. Instead, in our case here, at $\kappa = \pi$ the potential appears already asymmetric with two energy wells having different depths, cf. Fig. 2(b). We associate this asymmetry with the finite injectors size, i.e., $\phi_{inj}(x)$ is not a sharp jump from 0 to κ, but rather a smooth function of x. From Eq. (4) the normalized Josephson-energy density term

$$u(\mu,x) = 1 - \cos[\mu - \phi_{inj}(x) + 2\pi f x]. \quad (5)$$

This is the Josephson energy per junction width w and λ_J normalized to $\Phi_0 j_c/(2\pi)$. For $f = 0$ it looks like the conventional $1 - \cos(\mu)$ and the shifted $1 - \cos(\mu - \kappa)$ profiles in the left and the right part of the JJ, respectively, see the background image in Fig. 3 corresponding to the $u(\mu,x)$ profile. Near the injectors the valleys (minima) are connected according to the $\phi_{inj}(x)$ dependence. One can see that at $\kappa = \pi$ the two phase solutions $\mu_\pm(x)$, see Fig. 3(a), are not in a symmetric situation. The $\mu_+(x)$ passes through the "canyon"—a low Josephson energy density (dark) region near the injectors, while the $\mu_-(x)$ solution passes through the "ridge"—a high energy Josephson energy density (light) region near the injectors. This explains why the total energy of the $+\varphi = \langle\mu_+(x)\rangle$ solution is lower than the one of the $-\varphi = \langle\mu_-(x)\rangle$ solution.

The asymmetry of $U(\psi)$ shown in Fig. 2(b) for $\kappa = \pi$ can be cured by increasing κ slightly over π. In this way we shift the cos-like energy profile in the right side of Fig. 3 further up (towards a larger phase) so that the $\mu_+(x)$ solution gets a larger phase difference $\mu_+(l/2) - \mu_+(-/2)$ and therefore a larger total energy, while the $\mu_-(x)$ solution gets a smaller phase difference $\mu_-(l/2) - \mu_-(-l/2)$ and therefore a smaller total energy. At some value κ_{sym} the energies $U(-\varphi) = U(+\varphi)$, see Fig. 2(c). A similar compensation can be obtained by applying a small magnetic flux f to the junction [see Fig. 2(d)]. For a finer tuning of the potential, κ and f can be changed simultaneously (not shown). The value of κ_{sym} seems to depend linearly on the effective injector size $w_{eff} = w_{inj} + w_d$, while it does not change with the injector location x_0 (provided x_0 is far from $\pm l/2$). In Figs. 2(c) and 2(d) yet another interesting feature of these junctions becomes evident: The energy minima do not simply occur at $\psi = \pm\varphi$, but at $\psi = \pm\varphi + \varphi_0$. This is not very surprising if one looks at Fig. 3. At κ_{sym}, the phase offset $\varphi_0 \propto \kappa_{sym} - \pi \propto w_{eff}$ and the two parameters are linked by the following equation $\varphi_0 = 0.5(\kappa_{sym} - \pi)$, provided x_0 is so small that we are in the double-well potential regime. The emergence of a finite φ_0 is thus related to the shift of κ from π to κ_{sym}.

Finally, in Fig. 2(e), we show that the height of the energy barrier U_0 separating the $\pm\varphi$ wells decreases as the injectors move away from the center of the junction. We observe that by varying the injectors position, together with κ to retain the symmetry of the potential, the two wells become more and more shallow with increasing x_0. Eventually, for $x_0 > x_c$, U_0 vanishes and one returns to the case of a single minimum. However, the minimum is shifted from zero [see Fig. 2(e)], i.e., we obtain a φ_0 JJ [24]. The value of x_c strongly depends on the length of the junction—the shorter l, the smaller x_c—as already pointed out in previous works [11,12,23,25] for a perfectly sharp discontinuity. Note that, if one is interested in the creation of a φ_0 JJ, this can be done even better by choosing κ away from $\kappa = \pi$, regardless of the value of x_0. In Fig. 3(c) we give an example by showing the phase $\mu(x)$ for the case $x_0 = 0.10$ and $\kappa = 0.68\pi$.

Below we use this model to numerically fit the experimental results. Possible discrepancies are to be explained considering

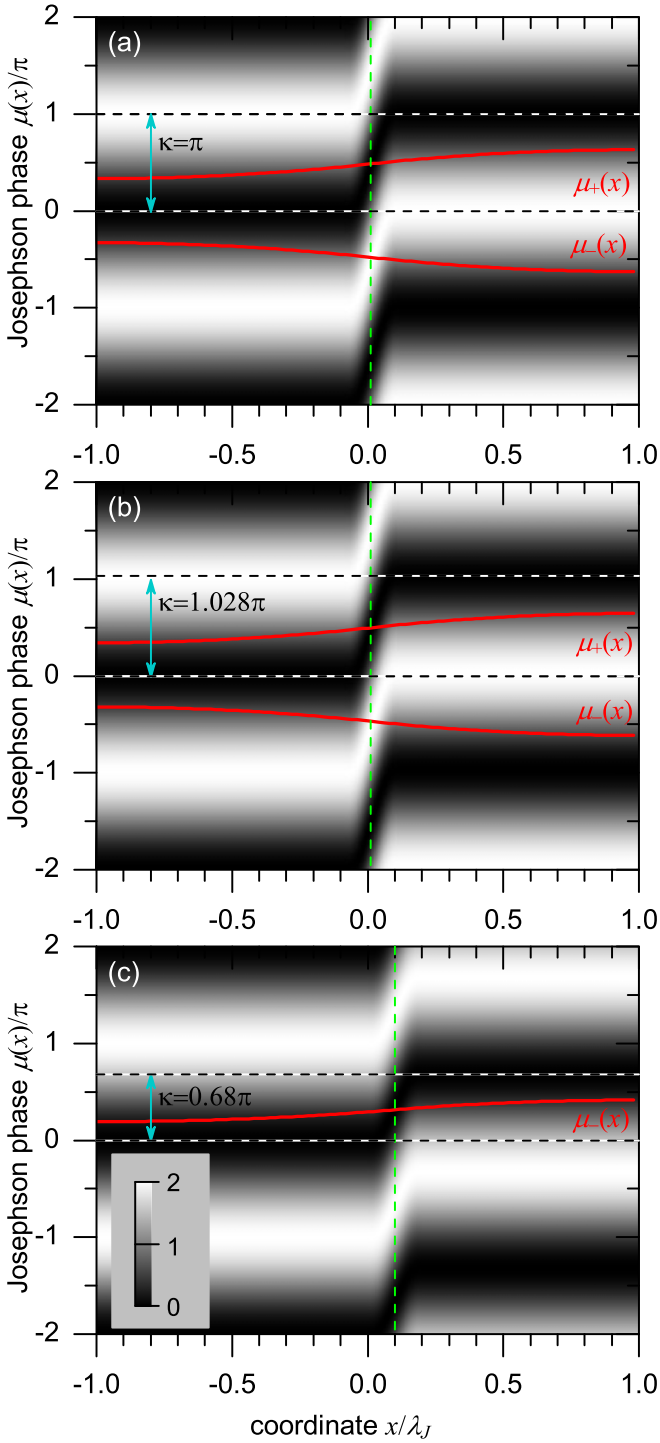

FIG. 3. Solutions $\mu(x)$ red lines on top of the grayscale plot $u(\mu,x)$ of the corresponding normalized Josephson energy density profile given by Eq. (5). The grayscale shows the range of u. (a) $x_0 = 0.02$ (vertical dashed line), $\kappa = \pi$; (b) $x_0 = 0.02$, $\kappa = \kappa_{\rm sym} = 1.028\pi$; (c) $x_0 = 0.10$, $\kappa = 0.68\pi$ ($\varphi_0 \approx 0.3\pi$ state). In all the plots, the normalized applied magnetic flux $f = 0$.

that the theory describes the simple geometry of a 1D junction with 1D injectors, while in real samples, we have 3D objects and the distribution of the currents applied to the junction and to the injectors may flow in a more complex way.

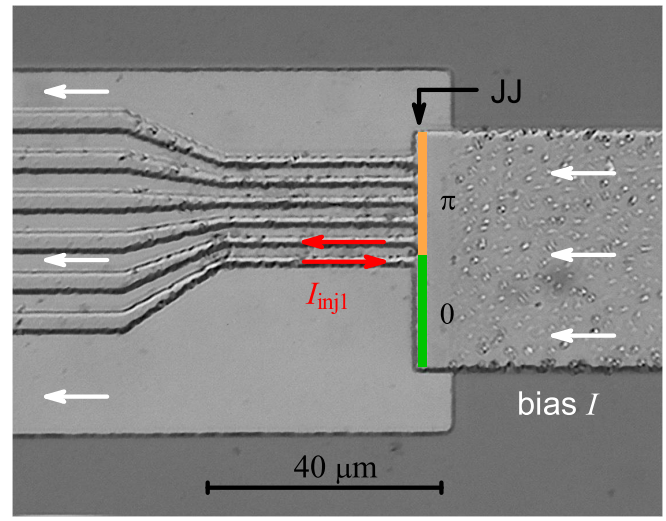

FIG. 4. Optical image of a JJ, for which the data are reported. It is equipped with three injector pairs, but only one of them, $I_{\rm inj1}$, was used for the experiment reported here.

III. EXPERIMENT

We fabricated Nb-AlO_x-Nb JJs with two injectors connected on the top electrode of the junction. The JJs have moderate length $L \sim 1.25...2.5\lambda_J$ and different width $W_{\rm inj} = 1$, 1.5 μm and position X_0 of the injectors [26]. In all our samples, $W_{\rm d} \simeq W_{\rm inj}$. A picture of one of the JJs is shown in Fig. 4. We have measured several junctions. The data presented in this paper were obtained on a junction with $L = 40$ μm, width $W = 0.8$ μm, $W_{\rm inj} = 1.5$ μm, and $X_0 \sim -0.125$ μm. The junction has the typical current-voltage (I-V) characteristic and dependence of I_c on the external magnetic field H of SIS JJs (both not shown), with $I_{\rm c} = 667$ μA at temperature $T = 4.2$ K. This corresponds to $j_{\rm c} \approx 2.08$ kA/cm^2 and $\lambda_J \approx 16$ μm [calculated from a numerical fit of $I_{\rm c}(H)$]. Thus, our JJ has a normalized length $l = 2.5\lambda_J$ and normalized injectors size $w_{\rm inj} \sim 0.09$.

A. Classical domain

Since the discontinuity κ is proportional to $I_{\rm inj}$, the critical current of the JJ modulates with $I_{\rm inj}$. In the case of δ injectors, this $I_{\rm c}(\kappa)$ [or equivalently $I_{\rm c}(I_{\rm inj})$] injectors calibration curve reaches the first minimum at $\kappa = \pi$, if the JJ is perfectly symmetric ($X_0 = 0$) and no self-field effect is present. The injectors calibration curve is symmetric for positive and negative bias, and the minimum corresponds to the formation of a φ JJ with a symmetric potential and $\varphi = \pm\pi/2$. For a JJ with $X_0 \neq 0$, the first minimum of the $I_c^+(I_{\rm inj})$ and $|I_c^-(I_{\rm inj})|$ curves [27] occur, instead, at different values of $I_{\rm inj}$. The injector current corresponding to $\kappa = \pi$ is centered between these values [23]. In the case of injectors with finite dimension, the calibration curve is analogous, however, as explained in Sec. II, the potential is expected to be symmetric at $\kappa_{\rm sym} > \pi$.

The experimental calibration curve of our junction is shown in Figs. 5(a) and 5(b). The first thing to notice here is that four critical currents (two for each bias polarity) appear around the first minimum of the curve. In addition, if we zoom in and

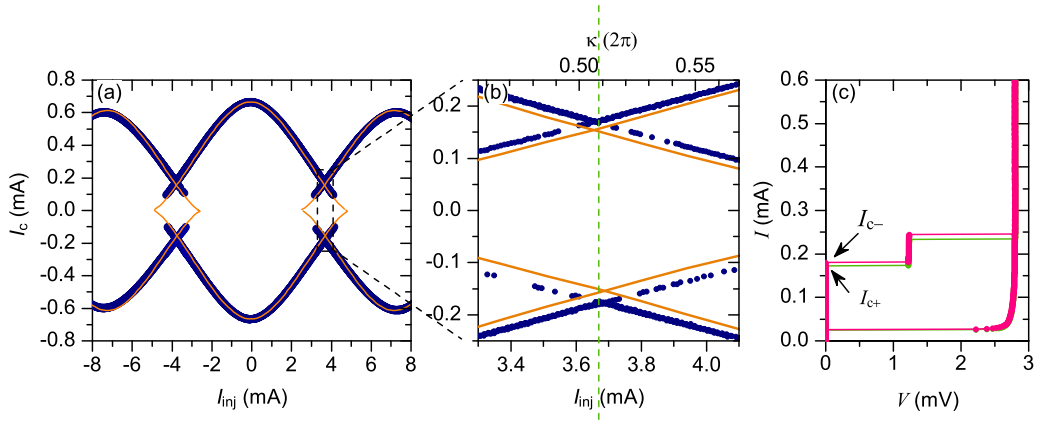

FIG. 5. (a) Experimental (blue line) and simulated (orange line) calibration of the injectors of a 40 μm long JJ with 1.5 μm wide injectors located at $X_0 = -0.125$ μm at $T = 4.2$ K and $H = 0$. In (b) a zoom around the first minimum is displayed. The dotted line indicates the value of κ (or I_{inj}) for which the potential has symmetric $\pm\varphi$ wells. (c) The I-V curve at $I_{inj}^{sym} = 3.67$ mA showing two distinct critical currents is plotted.

inspect more carefully, we observe a tiny asymmetry between the positive and negative bias curves [see Fig. 5(b)]. The dotted line in Fig. 5(b) indicates the value of $I_{inj} = I_{inj}^{sym} = 3.67$ mA where the Josephson potential is symmetric, i.e., $I_{c\pm}^{+} = |-I_{c\pm}^{-}|$. From the comparison with the simulated curve, cf. Fig. 5(b), we can estimate $\kappa_{sym} = 1.042\pi$. The value of I_{inj}^{sym} changes slightly with temperature; at $T = 20$ mK we measured $I_{inj}^{sym} = 3.71$ mA.

Figure 5(c) shows the I-V curve measured for $I_{inj}^{sym} = 3.67$ mA. By applying the bias current using special sweep sequences [10], we were able to detect the two critical currents I_{c-} and I_{c+}. The two currents are also observable in the $I_c(H)$ dependence, where a characteristic minimum around $H = 0$ appears (not shown), as we know from Ref. [11]. In our previous work, where we used the SIFS-based φ JJ, the high damping prevented us from observing two critical currents at $T = 4.2$ K. In the present junctions, instead, the damping is very low and two critical currents are measurable in a wide range of temperatures.

B. Quantum domain

Further we investigated the phase escape from the double well potential of the φ JJ. For this, we have cooled down our sample in a dilution refrigerator and performed measurements in a temperature range from 20 mK to 600 mK. To reduce the noise the dilution fridge has RC filters, π filters, and powder filters at different stages. We have collected statistics of switching currents at $I_{inj}^{sym} = 3.71$ mA by sweeping the bias current with a constant ramp rate $\dot{I} = 79.6$ mA/s, recording the value of the switching current during each sweep. By repeating such measurements $N = 5000$ times, we were able to plot histograms of switching current distributions. Since at low damping the initial state ($-\varphi$ or $+\varphi$) is random [2,3], we obtain histograms containing two peaks corresponding to I_{c-} and I_{c+}, as shown in Fig. 6(a). As the temperature decreases, each peak shifts towards the noise-free critical current $I_{c0\pm}$ and the width of the histogram decreases. The dependence of the width $\sigma_{\pm}(T)$ of each peak is extracted from the experimental data and presented in Fig. 6(b). One clearly sees that both

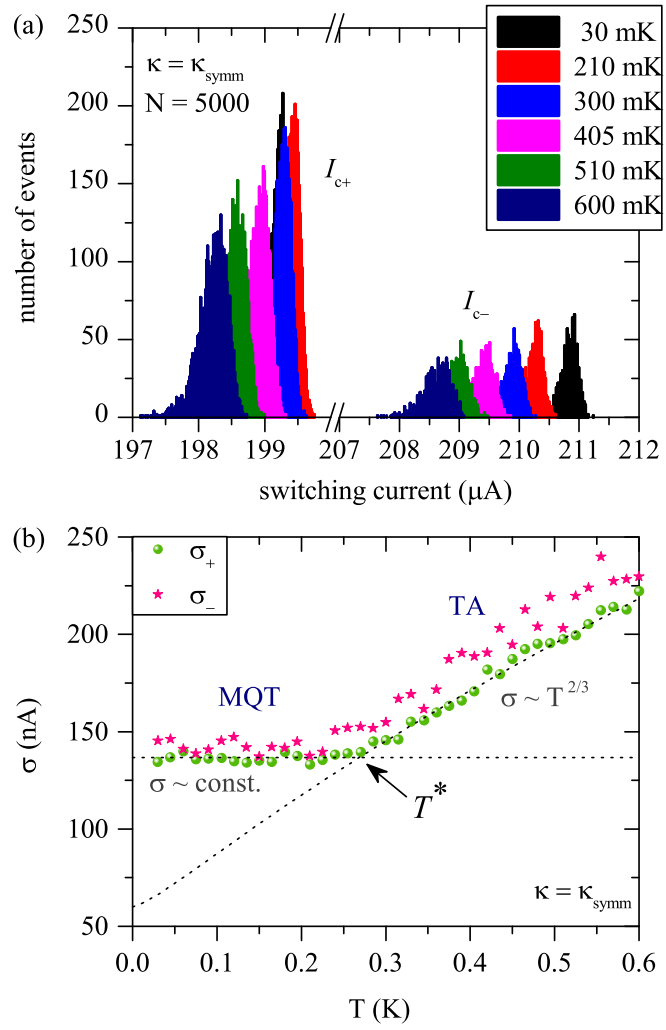

FIG. 6. (a) Several switching current histograms taken at $I_{inj}^{sym} = 3.71$ mA and at different temperatures. Each histogram has two peaks corresponding to the escape from the $-\varphi$ and the $+\varphi$ well. Each peak is somewhat below I_{c0+} and I_{c0-}, the fluctuation-free critical currents of the φ JJ. (b) The widths $\sigma_{\pm}$ of the I_{c-} and I_{c+} peaks in (a) as a function of temperature T is shown.

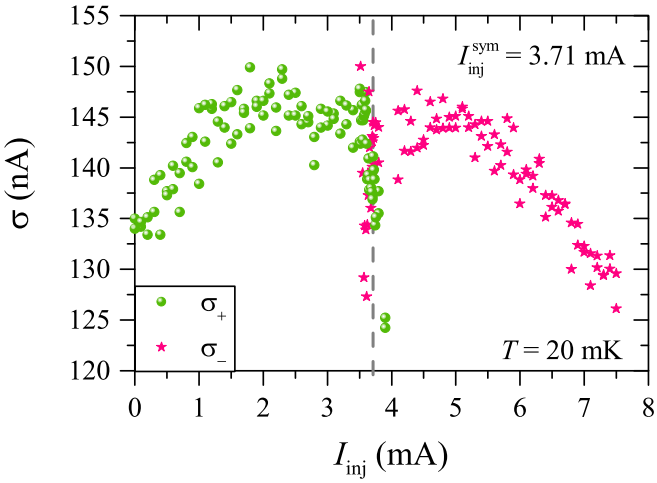

FIG. 7. The dependences $\sigma_{\pm}(\kappa)$ at $T = 20$ mK. The dotted line indicates the symmetry point occurring at $I_{inj}^{sym} = 3.71$ mA.

$\sigma_{\pm}(T)$ saturate at $T < T^{\star} \approx 260$ mK at values $\sigma_{+}^{sat} \approx 137$ nA and $\sigma_{-}^{sat} \approx 142$ nA. Such a saturation of the escape peak width is evidence of the crossover from the thermal escape of the phase to the macroscopic quantum tunneling of the phase out of the $-\varphi$ or $+\varphi$ well.

However, one should be extremely careful with such conclusions, since the saturation might be caused (a) by the parasitic heating of the sample to a temperature above the bath temperature due to temporary switching to the resistive state or (b) by some background noise in our experimental setup, which has little to do with MQT. There can be several types of such noise: (i) constant background noise picked up from the environment because some wires work as an antenna; (ii) noise in the bias current circuit with $\sigma_b = c_0 + c_1 I$; (iii) noise in the injector circuit with $\sigma_{inj} \propto I_{inj}$. To rule out overheating, we have repeated our measurements using different duty cycles and different ramp rates and observed no qualitative difference.

The standard technique to exclude the saturation due to electronic noise is to demonstrate that in the used setup one can measure σ values, which are below $\sigma_{\pm}^{sat}$, possibly in the same experiment and with the same sample. Already from Fig. 6(b) one can conclude that σ_{-}^{sat} is *not* due to the background noise because we have measured a smaller value of σ_{+}^{sat} at the same I_{inj}. Nevertheless, if the noise is $\propto I$, one can easily observe such σ_{-}^{sat} as $I_{c-} > I_{c+}$. An analysis of the $\sigma(I_c)$ dependence suggests that this is not the case in our measurements, since $\sigma_{\pm}(I_c)$ stays approximatively constant when I_c is modulated by the injector current, see Fig. 7. Moreover, we can exclude significant contribution of random noise in the bias circuit as, for $T < T^{\star}$, the dependences of the skewness (S) and kurtosis (K) of escape histograms on I_c are constant and they tend to the universal values of $S = -1$ and $K = 5$ [28].

In MQT experiments with conventional small JJs, one usually changes some parameter, e.g., one applies a magnetic field, in order to decrease the effective I_c and, accordingly [29], the histogram width $\sigma \propto I_c^{3/5}$. In our system the tuning parameter is κ, therefore we have measured $\sigma_{\pm}^{sat}(I_{inj})$ at $T = 20$ mK, see Fig. 7. The dependence is almost symmetric with respect to the value $I_{inj}^{sym} = 3.71$ mA. One can see that both σ_{+}^{sat} and σ_{-}^{sat} have a maximum at $\kappa \approx \pi$ and that our setup is able to measure values of σ as low as 130 nA. The presence of points (κ values) where $\sigma_{\pm} < \sigma_{\pm}^{sat}$ automatically means that at all other values of κ, where $\sigma_{\pm}$ is larger, we *do not* observe saturation due to noise. Also, if the noise would be caused by I_{inj}, one would observe its monotonous increasing component as $\kappa \propto I_{inj}$ grows. Figure 7 clearly shows that this is *not* the case. The higher moments $S(I_{inj}) \approx -1$ and $K(I_{inj}) \approx 5$ confirm also absence of white noise contributions. We conclude that we indeed observe MQT.

The presence of some background noise of nonthermal origin is nevertheless obvious. One can see that the extrapolation of the $\sigma_{\pm}{}^2(T) = [\sigma_{bg}^2 + (\eta \cdot T^{2/3})^2]$ dependence, shown in Fig. 6(b), from the thermal escape region (with $\eta = 295$ nA K$^{3/2}$) towards $T \to 0$, results in $\sigma_{bg} \approx 60$ nA, which can be taken as a reasonable estimate of the parasitic noise level in our system.

Additional indications of the quantum behavior of the phase in our φ JJ can be found in the analysis of the escape rate Γ as a function of the bias current. For the computation of the experimental Γ for each switching current peak in Fig. 6(a) we have used the formula [30]

$$\Gamma_{\pm}(I_k) = \frac{\dot{I}}{\Delta I} \ln \frac{\sum_{j=k}^{M} P(I_j)}{\sum_{j=k+1}^{M} P(I_j)}, \tag{6}$$

where M is the number of bins of width ΔI of the built histogram and $P(I_j)$ is the discretized probability distribution of the switching current. The results are compared to the theoretical expectations for the thermal activation (TA) and the MQT regime, which, in the low-to-moderate damping limit, are, respectively, given by [31,32]

$$\Gamma_t(I) = a_t \frac{\omega_p}{2\pi} \exp\left(- \frac{\Delta U}{k_B T} \right), \tag{7}$$

$$\Gamma_q(I) = a_q \frac{\omega_p}{2\pi} \exp\left(- 7.2 \frac{\Delta U}{\hbar \omega_p} \right), \tag{8}$$

where a_t and a_q are damping-dependent prefactors, $\omega_p(I) = P_{\omega_0}(1 - I/I_{c0})^{1/4}$ is the plasma frequency, and $\Delta U = P_{\Delta U}(1 - I/I_{c0})^{3/2}$ is the energy barrier. P_{ω_0} and $P_{\Delta U}$ are the plasma frequency and the energy barrier prefactors for a JJ with two degenerate ground states. The expression and the theoretical study of such parameters are given in Ref. [23]. By explicating the current dependence of all parameters in the exponent of Eq. (7) and Eq. (8), one obtains $\Gamma_t, \Gamma_q \sim \exp[(1 - I/I_{c0})^m]$, where $m = 3/2$ in the thermal regime and $m = 5/4$ in the quantum regime.

To perform the comparison, we first plotted the quantity $[\ln(\omega_p/2\pi\Gamma_{\pm})]^{1/m}$ versus the switching current I for a few temperatures in the range from 600 to 30 mK. In such a way, one gets a linear function and the noise-free current $I_{c0\pm}$ can be extrapolated from the intercept with the current axis. We iteratively fitted the experimental data with a weighted linear least-square fit in order to have a precise estimation of $I_{c0\pm}$. For the sake of simplicity, in our procedure we adopted $a_t, a_q = 1$. Subsequently, we graphed the double logarithm of the normalized inversed escape rate $\omega_p/2\pi\Gamma_{\pm}$ as a function of $\ln(1 - I/I_{c0})$, that is again a linear function. The choice of the double-log plot has been made in order to highlight

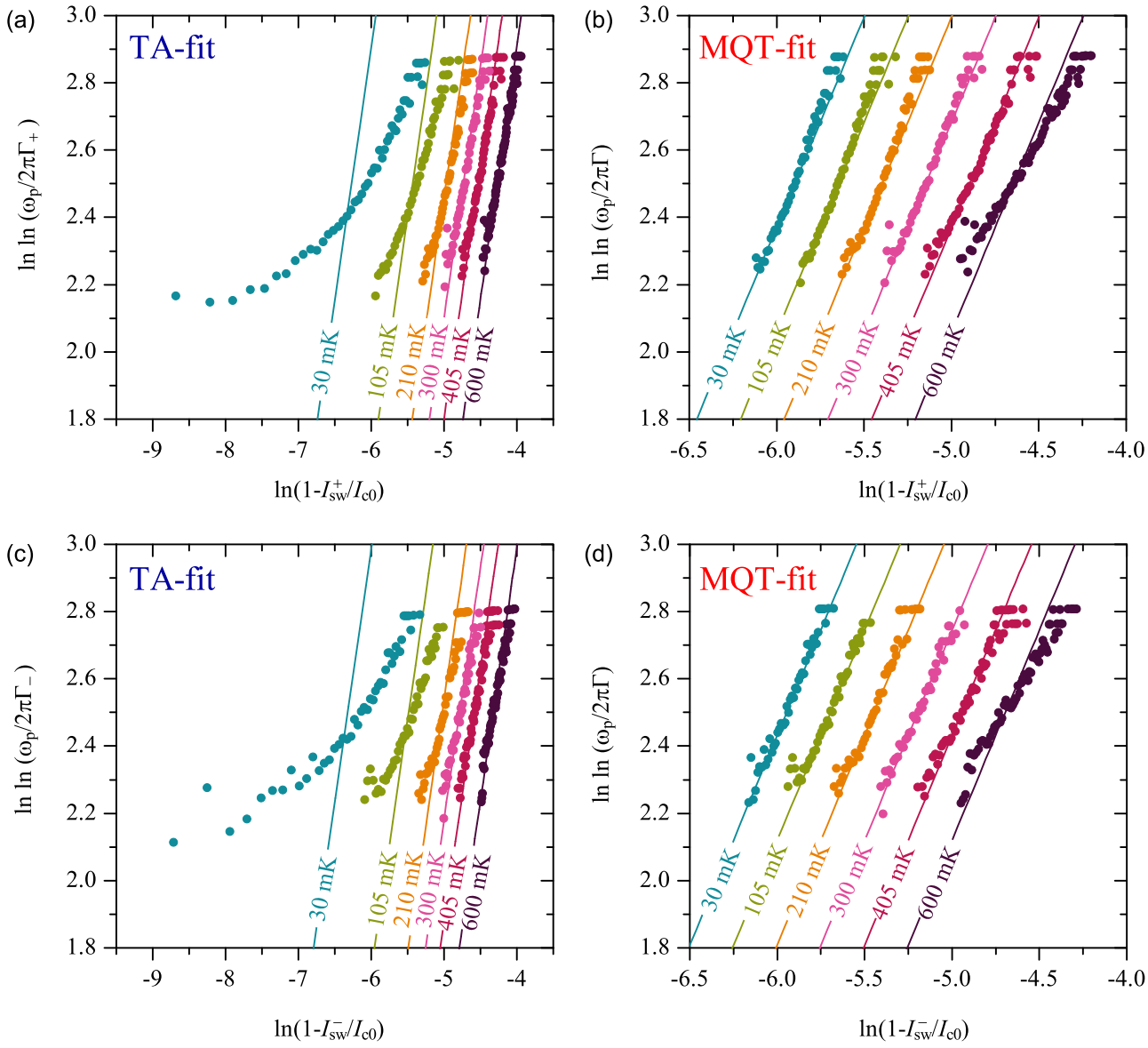

FIG. 8. Double logarithm of the normalized inverse escape rate $\ln\ln(\omega_p/2\pi\,\Gamma)$ for different temperatures in the range 30 mK $< T <$ 600 mK for the I_{c+} peak of Fig. 6(a) [panels (a) and (b)] and for the I_{c-} peak of Fig. 6(a) [panels (c) and (d)]. In the graphs, the points represent the experimental data and the lines the fits obtained by using Eq. (7) (TA-fit) and Eq. (8) (MQT-fit). One can clearly observe that for both peaks (both energy wells $\pm\varphi$) the TA formula fits very well the experimental points above $T^\star$, but it does not below $T^\star$. The opposite occurs for the MQT formula, proving quantum tunneling below the crossover, where the standard deviations $\sigma_\pm$ saturate. In panels (b) and (d), the curves were manually shifted by -0.5 to display them better. Since there is no dependence on temperature in Γ_q, the curves sit almost at the same position in the diagram.

the difference in the slopes m of the thermal and quantum formulas. Our results are displayed in Fig. 8 for both the right and left peak of Fig. 6(a). In Figs. 8(a) and 8(c), we fitted the data using the thermal formula for the escape rate [Eq. (7)], while in (b) and (d) we used the quantum expression [Eq. (8)]. What is evident here is that, for both peaks, Γ_t matches the experimental points perfectly for $T > T^\star$, but it deviates significantly for $T < T^\star$. The experimental escape below $T^\star$ is fitted very well by Γ_q, which in turn fails for higher temperature. This analysis lends further support to the claim that below the crossover temperature the escape mechanism in our junction is dominated by quantum tunneling of the phase. Note that the assumption of $a_t = 1$ and $a_q = 1$ does not affect the latter result, since the prefactors logarithmically enter into the escape rate computation.

IV. CONCLUSIONS

In conclusion, we have demonstrated a φ JJ realized using a phase discontinuity κ created in a SIS JJ by two tiny current injectors of finite size and investigated the quantum properties of such a φ JJ. We have described the system theoretically and have shown simulations of the Josephson energy potential taking into account the finite size of the injectors. We have shown that such a JJ can be turned from a 0 JJ to a $\varphi_0 \pm \varphi$ JJ by simply varying the amplitude of the current $I_{\rm inj}$ flowing through

the injectors. Additionally, one can obtain a φ_0 JJ if the injectors are located far away from the center of the junction or if κ is not near $\kappa_{\rm sym}$. We have demonstrated such a tunable device experimentally by giving clear evidence of the $\pm\varphi$ states. The predicted φ_0 shift of the phase in the ground state could not be proven or estimated, since this requires a phase-sensitive setup.

Furthermore, simulations show that by changing the position of the injectors along the length of the junction, the energy barrier U_0 between the $\pm\varphi$ wells decreases down to values of the order of $10^{-4}E_J$, which is interesting if one wants to perform measurements to study macroscopic quantum coherence between the $-\varphi$ and $+\varphi$ states. Nevertheless, the approach with two injectors is not very suitable for such an operation. In order to have very shallow and symmetric wells, the position of the injectors and the values of the applied $I_{\rm inj}$ have to be controlled with high precision [11,12,23,25]. To solve this problem, one can use more injectors, see Fig. 4, to electronically fine tune the potential. Details will be given elsewhere. Another approach is to use a 0-π SQUID instead of 0-π continuous junction. In the 0-π SQUID the effective double-well potential is less sensitive to the parameter spread [33].

Finally, we have performed quantum mechanical experiments of the Josephson phase escape and provided evidence of macroscopic quantum tunneling of the average phase ψ from *both* minima $\pm\varphi$ of the Josephson potential. The thermal to MQT crossover temperature occurring at $T^\star \approx 260$ mK is indicated by the saturation of the widths $\sigma_\pm(T)$ of the histograms for the switching currents I_{c-} and I_{c+}. We exclude the possible influence of background noise in our system, since we could measure values of $\sigma_\pm$ lower than $\sigma_\pm^{\rm sat}$. Further proofs of MQT are given by fitting the escape rates from both wells using MQT and TA formulas. The fits show that thermal activation is the dominant escape process above $T^\star$, while quantum tunneling prevails below $T^\star$.

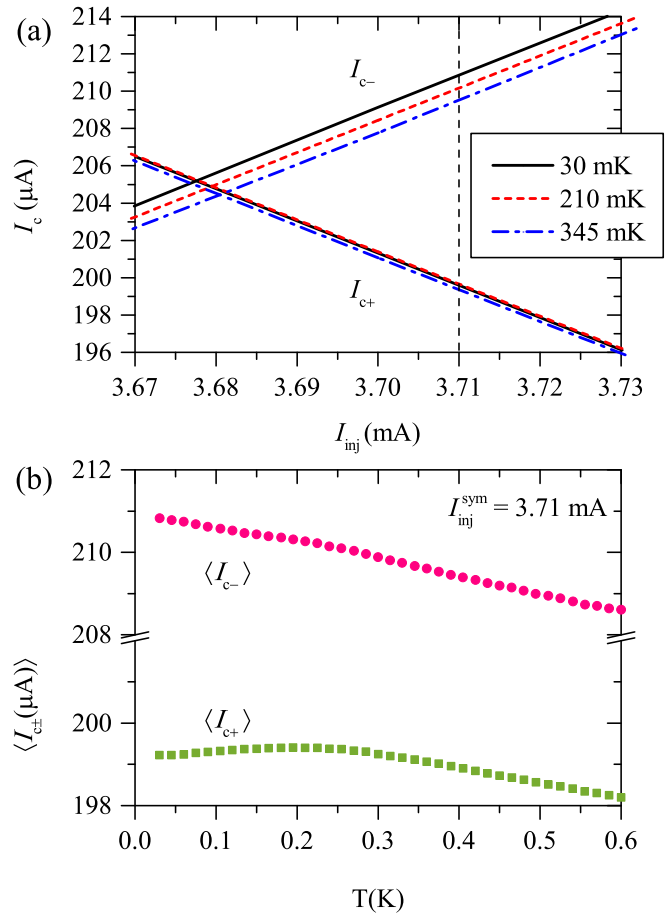

FIG. 9. (a) Modulation of the critical current I_c with injector current $I_{\rm inj}$ at different temperatures. The vertical line indicates $I_{\rm inj}^{\rm sym} = 3.71$ mA. (b) Mean switching currents vs temperature at $I_{\rm inj}^{\rm sym} = 3.71$ mA.

ACKNOWLEDGMENTS

We thank A. Ustinov and I. Pop for useful discussions. R.M. gratefully acknowledges support by the Carl Zeiss Stiftung. This work was funded by the Deutsche Forschungsgemeischaft (DFG) via Projects No. GO-1106/5 and No. SFB/TRR 21 A5. We also acknowledge support by the European Cooperation in Science and Technology (COST) action NANOCOHYBRI (CA16218).

APPENDIX

The histograms in Fig. 6(b) exhibit an unexpected temperature dependence. The left peak corresponding to I_{c-} moves to higher values of current as T is lowered, up to $T = 120$ mK, when it moves back. In order to understand the source of such an anomaly, we measured the $I_c(I_{\rm inj})$ dependence at different temperatures. As visible in Fig. 9(a), starting from $T = 30$ mK and increasing T, the minimum of the $I_c(I_{\rm inj})$ curve shifts to the right and decreases in value. Nevertheless, the symmetry point $I_{\rm inj}^{\rm sym}$ remains unvaried [vertical dotted line in Fig. 9(a)]. As a consequence, the critical current I_{c-} moves to lower values, whereas I_{c+}, first, raises slightly reaching a shallow maximum at $T \approx 210$ mK and then sinks. Thus, the ways the two currents change in temperature is different, as plotted in Fig. 9(b).

We suppose that this anomaly might be due to the geometry of our JJ. Our device has actually three injector pairs, as shown in Fig. 4. However, only the first one ($I_{\rm inj1}$) was used. The additional pairs ($I_{\rm inj2}, I_{\rm inj3}$) were not connected. Nevertheless, their presence makes the right and left halves of the junction different, e.g., the capacitances are higher in one side than in the other. The asymmetry in the geometry of the device may cause unusual temperature dependence of some quantities, e.g., $I_{c\pm}(T)$.

[1] E. Goldobin, D. Koelle, R. Kleiner, and A. Buzdin, Josephson junctions with second harmonic in the current-phase relation: Properties of φ junctions, Phys. Rev. B **76**, 224523 (2007).

[2] E. Goldobin, R. Kleiner, D. Koelle, and R. G. Mints, Phase Retrapping in a Pointlike φ Josephson Junction: The Butterfly Effect, Phys. Rev. Lett. **111**, 057004 (2013).

[3] R. Menditto, H. Sickinger, M. Weides, H. Kohlstedt, M. Žonda, T. Novotný, D. Koelle, R. Kleiner, and E. Goldobin, Phase retrapping in a φ Josephson junction: Onset of the butterfly effect, Phys. Rev. B **93**, 174506 (2016).

[4] T. Ortlepp, Ariando, O. Mielke, C. J. M. Verwijs, K. F. K. Foo, H. Rogalla, F. H. Uhlmann, and H. Hilgenkamp, Flip-flopping fractional flux quanta, Science **312**, 1495 (2006).

[5] A. K. Feofanov, V. A. Oboznov, V. V. Bol'ginov, J. Lisenfeld, S. Poletto, V. V. Ryazanov, A. N. Rossolenko, M. Khabipov, D. Balashov, A. B. Zorin, P. N. Dmitriev, V. P. Koshelets, and A. V. Ustinov, Implementation of superconductor/ferromagnet/superconductor π-shifters in superconducting digital and quantum circuits, Nat. Phys. **6**, 593 (2010).

[6] In general, the development of Josephson memory and switches attracts a lot of attention [34–39]. However, all cited devices store information by the magnetization of a ferromagnetic layer, while in the φ JJ the information is stored in two phase states $\pm\varphi$ and no remagnetization takes place.

[7] E. Goldobin, H. Sickinger, M. Weides, N. Ruppelt, H. Kohlstedt, R. Kleiner, and D. Koelle, Memory cell based on a φ Josephson junction, Appl. Phys. Lett. **102**, 242602 (2013).

[8] R. Menditto, H. Sickinger, M. Weides, H. Kohlstedt, D. Koelle, R. Kleiner, and E. Goldobin, Tunable φ Josephson junction ratchet, Phys. Rev. E **94**, 042202 (2016).

[9] P. Hänggi and F. Marchesoni, Artificial Brownian motors: Controlling transport on the nanoscale, Rev. Mod. Phys. **81**, 387 (2009).

[10] H. Sickinger, A. Lipman, M. Weides, R. G. Mints, H. Kohlstedt, D. Koelle, R. Kleiner, and E. Goldobin, Experimental Evidence of a φ Josephson Junction, Phys. Rev. Lett. **109**, 107002 (2012).

[11] E. Goldobin, D. Koelle, R. Kleiner, and R. G. Mints, Josephson Junction with a Magnetic-Field Tunable Ground State, Phys. Rev. Lett. **107**, 227001 (2011).

[12] A. Lipman, R. G. Mints, R. Kleiner, D. Koelle, and E. Goldobin, Josephson junctions with tunable current-phase relation, Phys. Rev. B **90**, 184502 (2014).

[13] N. G. Pugach, E. Goldobin, R. Kleiner, and D. Koelle, Method for reliable realization of a φ Josephson junction, Phys. Rev. B **81**, 104513 (2010).

[14] N. Ruppelt, H. Sickinger, R. Menditto, E. Goldobin, D. Koelle, R. Kleiner, O. Vavra, and H. Kohlstedt, Observation of 0-π transition in SIsFS Josephson junctions, Appl. Phys. Lett. **106**, 022602 (2015).

[15] A. V. Ustinov, Fluxon insertion into annular Josephson junctions, Appl. Phys. Lett. **80**, 3153 (2002).

[16] B. A. Malomed and A. V. Ustinov, Creation of classical and quantum fluxons by a current dipole in a long Josephson junction, Phys. Rev. B **69**, 064502 (2004).

[17] E. Goldobin, A. Sterck, T. Gaber, D. Koelle, and R. Kleiner, Dynamics of Semifluxons in Nb Long Josephson 0-π Junctions, Phys. Rev. Lett. **92**, 057005 (2004).

[18] T. Gaber, E. Goldobin, A. Sterck, R. Kleiner, D. Koelle, M. Siegel, and M. Neuhaus, Nonideal artificial phase discontinuity in long Josephson 0-κ junctions, Phys. Rev. B **72**, 054522 (2005).

[19] M. Beck, E. Goldobin, M. Neuhaus, M. Siegel, R. Kleiner, and D. Koelle, High-Efficiency Deterministic Josephson Vortex Ratchet, Phys. Rev. Lett. **95**, 090603 (2005).

[20] M. Knufinke, K. Ilin, M. Siegel, D. Koelle, R. Kleiner, and E. Goldobin, Deterministic Josephson vortex ratchet with a load, Phys. Rev. E **85**, 011122 (2012).

[21] K. Buckenmaier, T. Gaber, M. Siegel, D. Koelle, R. Kleiner, and E. Goldobin, Spectroscopy of the Fractional Vortex Eigenfrequency in a Long Josephson 0-κ Junction, Phys. Rev. Lett. **98**, 117006 (2007).

[22] A. Dewes, T. Gaber, D. Koelle, R. Kleiner, and E. Goldobin, Semifluxon Molecule Under Control, Phys. Rev. Lett. **101**, 247001 (2008).

[23] E. Goldobin, S. Mironov, A. Buzdin, R. G. Mints, D. Koelle, and R. Kleiner, Effective model for a short Josephson junction with a phase discontinuity, Phys. Rev. B **93**, 134514 (2016).

[24] A. Buzdin, Direct Coupling Between Magnetism and Superconducting Current in the Josephson φ_0 Junction, Phys. Rev. Lett. **101**, 107005 (2008).

[25] A. Buzdin and A. E. Koshelev, Periodic alternating 0- and π-junction structures as realization of ϕ-Josephson junctions, Phys. Rev. B **67**, 220504(R) (2003).

[26] J. M. Meckbach, M. Merker, S. J. Buehler, K. Ilin, B. Neumeier, U. Kienzle, E. Goldobin, R. Kleiner, D. Koelle, and M. Siegel, Sub-μm Josephson junctions for superconducting quantum devices, IEEE Trans. Appl. Supercond. **23**, 1100504 (2013).

[27] The superscripts '+' and '−' refer to the polarity of the corresponding current. So $|I_c^-(I_{\rm inj})| \neq I_c^+(I_{\rm inj})$.

[28] A. Murphy, P. Weinberg, T. Aref, U. C. Coskun, V. Vakaryuk, A. Levchenko, and A. Bezryadin, Universal Features of Counting Statistics of Thermal and Quantum Phase Slips in Nanosize Superconducting Circuits, Phys. Rev. Lett. **110**, 247001 (2013).

[29] A. Garg, Escape-field distribution for escape from a metastable potential well subject to a steadily increasing bias field, Phys. Rev. B **51**, 15592 (1995).

[30] T. A. Fulton and L. N. Dunkleberger, Lifetime of the zero-voltage state in Josephson tunnel junctions, Phys. Rev. B **9**, 4760 (1974).

[31] H. A. Kramers, Brownian motion in a field of force and the diffusion model of chemical reactions, Physica (Utrecht) **7**, 284 (1940).

[32] A. O. Caldeira and A. J. Leggett, Quantum tunneling in a dissipative system, Ann. Phys. **149**, 374 (1983).

[33] E. Goldobin, D. Koelle, and R. Kleiner, Tunable $\pm\varphi$, φ_0, and $\varphi_0 \pm \varphi$ Josephson junction, Phys. Rev. B **91**, 214511 (2015).

[34] B. Baek, W. H. Rippard, S. P. Benz, S. E. Russek, and P. D. Dresselhaus, Hybrid superconducting-magnetic memory device using competing order parameters, Nat. Commun. **5**, 3888 (2014).

[35] M. Abd El Qader, R. K. Singh, Sarah N. Galvin, L. Yu, J. M. Rowell, and N. Newman, Switching at small magnetic fields in Josephson junctions fabricated with ferromagnetic barrier layers, Appl. Phys. Lett. **104**, 022602 (2014).

[36] T. Golod, A. Iovan, and V. M. Krasnov, Single Abrikosov vortices as quantized information bits, Nat. Commun. **6**, 8628 (2015).

[37] E. C. Gingrich, B. M. Niedzielski, J. A. Glick, Y. Wang, D. L. Miller, R. Loloee, W. P. Pratt Jr, and N. O. Birge, Controllable 0-π Josephson junctions containing a ferromagnetic spin valve, Nat. Phys. **12**, 564 (2016).

[38] R. Caruso, D. Massarotti, V. V. Bolginov, A. Ben Hamida, L. N. Karelina, A. Miano, I. V. Vernik, F. Tafuri, V. V. Ryazanov, O. A. Mukhanov, and G. P. Pepe, RF assisted switching in magnetic Josephson junctions, J. Appl. Phys. **123**, 133901 (2018).

[39] I. M. Dayton, T. Sage, E. C. Gingrich, M. G. Loving, T. F. Ambrose, N. P. Siwak, S. Keebaugh, C. Kirby, D. L. Miller, A. Y. Herr, Q. P. Herr, and O. Naaman, Experimental demonstration of a Josephson magnetic memory cell with a programmable π-junction, IEEE Mag. Lett. **9**, 3301905 (2018).